ARTICLE

First-Principles Studies on Oxygen-Induced Faceting of Ir(210)

Payam Kaghazchi,[†] Timo Jacob,[†,*] Ivan Ermanoski,[‡] Wenhua Chen,[‡] and Theodore E. Madey[‡]

[†]Fritz-Haber-Institut der Max-Planck-Gesellschaft, Faradayweg 4-6, D-14195 Berlin, Germany, and Rutgers University, Piscataway, New Jersey 08854, and [‡]Department of Physics and Astronomy and Laboratory of Surface Modification, Rutgers, The State University of New Jersey, 136 Frelinghuysen Road, Piscataway, New Jersey 08854

ABSTRACT Density functional theory calculations were performed to obtain an atomistic understanding of facet formation on Ir(210). We determined geometries and energetics of clean and oxygen-covered surfaces of planar Ir(210) as well as Ir(311) and two types of Ir(110) surfaces, which are involved in faceting by forming three-sided nanopyramids. Using the energies together with the *ab initio* atomistic thermodynamics approach, we studied the stability of substrate and facets in the presence of an oxygen environment. Our results show that facets are stable over the entire temperature range at which oxygen is adsorbed on the surface at coverages ≥0.45 physical ML, supporting the picture of a thermodynamic driving force. We also investigated the dependence of the phase diagram on the choice of the exchange-correlation functional and obtained qualitatively the same behavior. Finally, this work helps to better understand reactivity and selectivity of O-covered planar and faceted Ir surfaces in catalysis.

KEYWORDS: density functional theory · iridium · oxygen · facet formation · surface · adsorption

Surface faceting can be understood as a morphology change from a planar surface to a hill-and-valley structure. While clean metal surfaces rarely facet, adsorbate-induced faceting of surfaces, driven by the anisotropy of surface free energy, is a general phenomenon observed in many systems.[1–3] Usually the facets have more close-packed surface structures than the original surface, resulting in a minimized surface free energy, although the total surface area may be increased. Studies of adsorbate-induced faceting can deepen our understanding of the stability of surfaces in contact with a reactive gas environment, which is essential for selecting and controlling a desired surface morphology. Faceted surfaces have also been used as model systems to study structural sensitivity in catalytic reactions[4–6] and may be used as templates to grow nanostructures.[7,8]

So far, adsorbate-induced faceting has been studied experimentally on various metal surfaces such as W(111),[1,2] Mo(111),[9,10] Ni(210),[11,12] Pt(210),[13] Ir(210),[14] Rh(553),[15] Re(11$\bar{2}$1) and Re(12$\bar{3}$1),[16,17] as well as vicinal Cu surfaces.[18–21] Although the enhancement of the anisotropy in surface free energy is the thermodynamic driving force for facet formation, in most cases, this process is hindered by kinetic limitations. Therefore, not only a critical adsorbate coverage is required but also a minimum annealing temperature, allowing the system to overcome all kinetic barriers in the process of facet formation.

Ermanoski *et al.* have recently found that O adsorption can induce faceting of Ir(210).[14,22] Starting with planar Ir(210), which is a relatively open surface, and depositing oxygen at coverages of $\theta > 0.5$ ML, they could produce three-sided nanopyramids by annealing the O-covered Ir(210) surface to temperatures higher than 600 K. Low energy electron diffraction (LEED) and scanning tunneling microscopy (STM) revealed that these facets, which completely covered the surface, expose faces of Ir(311), Ir(31$\bar{1}$), and Ir(110). Furthermore, higher resolution STM images showed that, while the (311) and (31$\bar{1}$) faces are always unreconstructed, some (110) faces are partially reconstructed. This superstructure was proposed to be a "stepped double-missing-row"-(110) surface.[23]

After facet formation, oxygen that still remains on the surface can be removed by reaction with H_2 at $T < 400$ K. During this reaction, the nanopyramidal surface structure is not affected since the kinetic barrier of facet destruction is not reached at these low temperatures. The clean nanofacets remain stable up to ~600 K, and for higher temperatures, the surface reverts to the original planar Ir(210).

By changing the annealing temperature for the formation of oxygen-covered faceted Ir(210), nanopyramids with average

*Address correspondence to jacob@fhi-berlin.mpg.de.

Received for review April 6, 2008 and accepted May 09, 2008.

Published online June 7, 2008. 10.1021/nn800210v CCC: $40.75

sizes ranging from 5 to 14 nm can be generated. Following oxygen removal, these surfaces provide unsupported monometallic substrates with well-defined structures and controlled sizes for studying size effects and structure sensitivity of catalytic reactions.[4–6]

After describing the thermodynamic procedure to evaluate the surface stabilities, we report calculations on the oxygen adsorption on Ir(210), (311), (110), and (110) superstructure surfaces. The obtained energies are then used with the *ab initio* atomistic thermodynamics approach to obtain the corresponding surface phase diagram. Finally, a short summary and future prospects is given.

THERMODYNAMIC CONDITION FOR FACET FORMATION

The energy required to form facets can be expressed as a sum of changes in the Gibbs free energies mainly related to surface, edge, kink, and strain contributions:

$$\Delta G^{\text{form}} = \Delta G^{\text{surface}} + \Delta G^{\text{edge}} + \Delta G^{\text{kink}} + \Delta G^{\text{strain}} + \ldots \quad (1)$$

When the size of the facets is large enough such that the overall contribution of step edges, kinks, and strain to the formation energy is rather small, it is reasonable to approximate the energy of formation by $\Delta G^{\text{surface}}$ only. On the basis of this condition (also called Herring condition), facet formation should occur when

$$\Delta G^{\text{form}} \approx \Delta G^{\text{surface}} = \sum_f A_f^{\text{final}} \gamma_f^{\text{final}} - A^{\text{initial}} \gamma^{\text{initial}} < 0 \quad (2)$$

which means that the system gains energy by transforming from an initial surface orientation with a surface free energy γ^{initial} and an overall area A^{initial} to a faceted surface, where the fth face is characterized by γ_f^{final} and A_f^{final}. Since, in our case, facets showing different faces are formed on the initially planar surface after adsorption of oxygen, eq 2 converts into the following condition, which has to be fulfilled in order to show facet formation:

$$\sum_f \frac{S_f}{\cos \vartheta_f} \gamma_f^{\text{final}}(T, p_{O_2}) < \gamma^{\text{initial}}(T, p_{O_2}) \quad (3)$$

where S_f specifies the partial contribution of face f to each pyramidal-shaped facet, while ϑ_f is the tilt angle of face f with respect to the initial substrate. In case of a fully faceted surface, S_f is the proportion of the surface covered by face f, such that the sum over S_f equals 1.

For the present case, where oxygen causes the formation of nanopyramids exhibiting {311} and (110) faces, eq 3 becomes

$$\frac{S_{311}}{\cos \vartheta_{311}} \gamma_{311}(T, p_{O_2}) + \frac{S_{110}}{\cos \vartheta_{110}} \gamma_{110}(T, p_{O_2}) < \gamma_{210}(T, p_{O_2}) \quad (4)$$

To evaluate the different surface free energies relevant in eq 4, the *ab initio* atomistic thermodynamics approach was used, which uses the condition that most relevant surface structures are characterized by a low surface free energy

$$\gamma(T, p_{O_2}) = \frac{1}{A}[G - N_{Ir}\mu_{Ir}^{\text{bulk}} - N_O \mu_O^{\text{gas}}(T, p_{O_2})] \quad (5)$$

where G is the Gibbs free energy of the particular slab, A the corresponding surface area, and μ_{Ir}^{bulk} and μ_O^{gas} are the chemical potentials of both reservoirs the system is assumed to be in contact with: Ir bulk and gaseous oxygen (O_2). Since the temperature and pressure dependence of all solid phases (surface and Ir bulk) is small compared to those of gaseous phases, the oxygen chemical potential, which is given by

$$\mu_O^{\text{gas}}(T, p_{O_2}) = \frac{1}{2}\left[E_{O_2}^{\text{tot}} + \bar{\mu}_{O_2}(T, p^0) + k_B T \ln\left(\frac{p_{O_2}}{p^0}\right)\right] \quad (6)$$

dominates the T and p dependence of the surface free energy γ. Here $E_{O_2}^{\text{tot}}$ is the DFT-calculated total energy of an isolated O_2 molecule and $\bar{\mu}_{O_2}(T, p^0)$ is the standard chemical potential that includes all contributions from vibrations and rotations of the molecule and the ideal gas entropy at 1 atm. Although the standard chemical potentials could be calculated from first principles, for the phase diagram that will be discussed later, we used the corresponding $\bar{\mu}_{O_2}(T, p^0)$ values from the JANAF thermodynamic tables.[29]

The Gibbs free energy G of the slab and the oxygen chemical potential have contributions from the internal energy U, configurational entropy, and vibrational free energy F^{vib}. The first contribution can be obtained from electronic structure DFT calculations. Since in the following we are only interested in relative stabilities, it is also reasonable to neglect contributions from configurational entropy.[30]

Following the approach described in ref 31 the vibrational contributions to γ coming from oxygen adsorption were estimated. At typical pressures of 5×10^{-11} atm, at which the faceting experiments were performed, and temperatures up to which oxygen is present on the surface ($T < \sim 1150$ K), we found these contributions to be rather small, leading to a slight temperature shift of <25 K only, but not causing any modifications in the ordering of surface phases. Therefore, in the following calculations, vibrational contributions have not been considered.

RESULTS AND DISCUSSION

In the following, we first discuss the adsorption of oxygen on the different surfaces that are involved in the facet formation, separately [Ir(210), (311), (110), and (110) superstructure; see Figures 1–4]; these were all generated on the basis of the calculated lattice con-

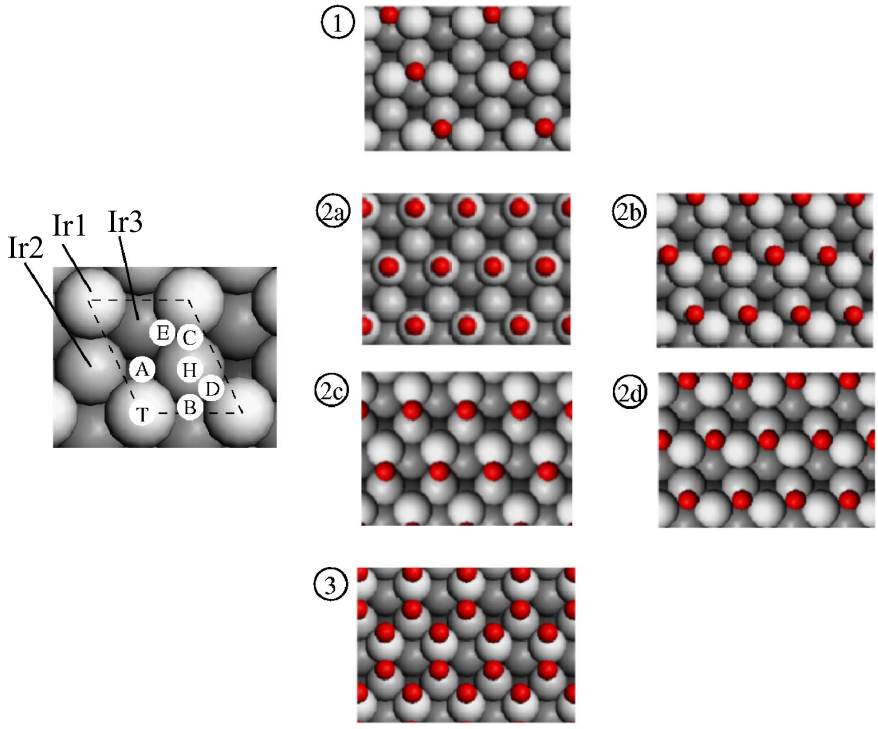

Figure 1. Top view of Ir(210) showing all binding sites at which O adsorption has been studied (left), as well as the most stable structures for different coverages (right): (1) 0.5 ML, (2a−d) 1 ML, (3) 2 ML.

stant of 3.90 Å (exptl[32] = 3.84 Å). The resulting binding energies are then used to generate the corresponding surface phase diagram for which we used the facet tilt angles (ϑ_f) and partial contributions to each pyramidal-shaped facet (S_f) as summarized in Table 1. Regarding the facets, two configurations are distinguished: (i) nanopyramids with (311), (31$\bar{1}$), and (110) regular faces, and (ii) and nanopyramids with (311), (31$\bar{1}$), and (110) superstructure faces, which both have been observed experimentally.

Although in previous calculations we found that for clean Ir(110) a (1 × 4) reconstruction is slightly more stable than the unreconstructed (1 × 1) surface,[31] the latter becomes more stable as soon as oxygen adsorbs. Since in the present work the (110) faces are only relevant for the nanofacets that form due to oxygen adsorption, in the following, we will not consider the reconstructed Ir(110) surface.

TABLE 1. Surface Area *A* per (1 × 1) Unit Cell (Calculated), Partial Surface Contributions (*S*), and Tilt Angles (ϑ) For Two Types of Nanopyramids: Those Consisting of (311) and (110) Faces and Those Consisting of (311) and (110) Superstructure Faces; For the Tilt Angles, Experimentally Measured and Geometrically Derived (Assuming Bulk-Truncated Unrelaxed Pyramids) Values Are Given (Taken from Ref 23)

surface	A (Å^2)	S	ϑ^{exp} (°)	ϑ^{geom} (°)
Ir(210)	17.00	–	–	–
Ir(311)	12.61	0.70	18.7 ± 0.7	19.29
Ir(110)	10.75	0.30	19.0 ± 0.9	18.43
Ir(311)	12.61	0.47	18.7 ± 0.7	19.29
Ir(110)-superstr.	82.24	0.53	7.0 ± 1.0	7.13

Since the surfaces studied here have different unit cell sizes, for our calculations, we use geometrical coverages θ, which are defined as the number of adsorbed oxygen atoms per (1 × 1) unit cell (see Figures 1–4) and vary with surface orientation. These are different than physical coverages often used experimentally, where adsorbate saturation is defined as 1 ML. While for Ir(110) regular and Ir(311) 1 geometrical ML is approximately 1 physical ML, for Ir(210), there is a 2:1 ratio (geom/phys),[33] and for Ir(110) superstructure, the conversion is approximately 8:1.

Figures 1–4 show probable (highly symmetric) binding sites, which were used as initial positions for the adsorbates, as well as the most stable adlayer configurations, for which the binding energies and bond distances are summarized in Table 2. All oxygen binding energies reported here are with respect to half a gas-phase oxygen molecule.

Ir(210)−0. We began our studies with DFT calculations on the adsorption of atomic oxygen on planar Ir(210) with coverages of θ = 0.5, 1, and 2 ML.

At 0.5 ML, we find that oxygen prefers binding at B-sites (see Figure 1-1) but slightly shifted toward the H position. This allows each adatom to form covalent bonds to two top-layer Ir atoms [d(Ir1−O) = 2.15 Å] and the nearby second-layer Ir atom [d(Ir2−O) = 2.10 Å], finally resulting in a three-fold binding. In this configuration, the binding energy per oxygen atom is 2.11 eV. The next stable binding sites are the T-site (BE = 1.78 eV) and C-site (BE = 1.76 eV), which are considerably less stable than the B-site. Moreover, we find that oxygen is not stable at A, D, E, and H positions and during geometry optimization moves to nearby positions: A → T, D → B, E → C, and H → B. For those sites, the adsorbates were first fixed in the x and y directions, and after preoptimizing the geometry, all constraints were removed in the final optimization procedure.

At a coverage of 1 ML, oxygen binds most strongly on top (T-site) of each first-layer Ir atom (BE = 1.78 eV) and at D-sites (BE = 1.76 eV), which allows the adsorbate to coordinate to two Ir surface atoms. Only slightly lower binding energies were obtained for the C-site (BE = 1.75 eV) and B-site (BE = 1.74 eV). At the remaining positions

TABLE 2. Binding Energies (Referenced to $^1/_2$ O_2), Sites, and Bond Lengths for Oxygen on Ir(210), Ir(311), Ir(110), and Ir(110) Superstructure Surfaces at Different Coverages; Only the Most Stable Structure for Each Coverage is Listed (The Ir−O Bond Lengths are as Labeled in Figures 1–4)

structure		coverage (ML)	binding site	E_{bind} (eV per $^1/_2$ O_2)	distances (Å)
Ir(210)		0.5	B	2.11	Ir1−O = 2.15, Ir2−O = 2.10
	Figure 1-2a	1.0	T	1.78	Ir−O = 1.80
	Figure 1-2b	1.0	D	1.76	Ir1−O = 1.96, Ir2−O = 2.06
	Figure 1-2c	1.0	C	1.76	Ir1−O = 1.92, Ir2−O = 2.06
	Figure 1-2d	1.0	B	1.74	Ir1−O = 2.24, Ir2−O = 2.05
		2.0	A/C	1.01	Ir1−O1 = 1.99, Ir2−O1 = 1.97
					Ir1−O2 = 1.83, Ir2−O2 = 3.26
Ir(311)	Figure 2-1a	0.5	A	2.16	Ir−O = 1.97
	Figure 2-1b	0.5	A	1.71	Ir−O = 1.98
		1.0	A	1.72	Ir−O = 1.98
Ir(110)		0.25	D	2.04	Ir−O = 1.97
		0.5	D	2.09	Ir−O = 1.97
		1.0	D	1.59	Ir−O = 1.99
Ir(110) superstructure		1.0	F	2.19	Ir1/Ir2−O = 1.98
		2.0	F/D	2.11	Ir1/Ir2−O1 = 1.98
					Ir3−O2 = 1.98
		3.0	F/F/D	1.96	Ir1−O1 = 2.06, Ir2−O1 = 1.94
					Ir3−O2 = 1.98
					Ir1−O3 = 2.06, Ir4−O3 = 1.94
		4.0	F/F/E/E	1.31	

(A, E, and H), oxygen is not stable and moves to nearby positions (A → T, E → C, and H → B). The similar binding energies for O on B-, D-, and T-sites result in a lower barrier for O diffusion along the -T-D-B-D-T- direction. This unusual 1D oxygen diffusion may be the key to the experimentally observed higher reactivity of Ir(210) for CO oxidation compared to that of faceted Ir(210), where the onset CO_2 desorption temperature is much lower on planar than that on faceted Ir(210).[6]

When the coverage is increased to 2 ML, a variety of oxygen overlayers could form. Using the position labeling of Figure 1, several possible combinations of distinguishable surface sites have been studied. Among these configurations occupying A and C (see Figure 1-3) leads to the highest binding energy (BE = 1.01 eV). In this configuration, the adatoms form a hexagonal-like structure. Interestingly, the A-site was found to be unstable at lower coverages (0.5 and 1 ML). This might explain the presence of two peaks in the low coverage regime of the O_2 TPD spectra (see O_2 TPD spectra for oxygen coverages ≤0.5 physical ML of Figure 2 in ref 14). There the peak temperatures are (roughly) 1200 and 950 K for 0.5 physical ML of O. However, it should be noted that at higher oxygen coverages (>0.5 physical ML) the low temperature peak shifts to a range between 780 and 900 K and therefore might be due to desorption from different faces of the faceted surface, since in this temperature range the surface already converts to the nanofaceted structure (due to higher oxygen coverage of >0.5 physical ML).

Ir(311)−0. Ir(311) oxygen coverages of 0.5 ML, having (1 × 2) or (2 × 1) periodicity as well as 1 ML with (1 × 1) periodicity, have been studied.

At θ = 0.5 ML, oxygen prefers binding at the A-site (bridge site) in a (1 × 2)-O adlayer structure (see Figure 2-1a) for which we calculated a binding energy per oxygen atom of 2.16 eV. In this configuration, the oxygen atom is 1.33 Å above the Ir surface plane (averaged over all Ir atoms in the topmost surface layer) with a Ir−O bond length of 1.97 Å. Induced by the presence of the strongly interacting adsorbates, there is a significant row-pairing of the topmost surface atoms, in which the Ir atoms, which are not bound to the same adatom, reduce their interatomic distance by 0.12 Å. This finally enables the oxygen atom to sit closer to the substrate. The next stable surface sites are the three-fold hollow F-site (BE = 1.59 eV), where oxygen binds to two top-layer and one second-layer Ir atoms and the on-top T-site (BE = 1.27 eV). In contrast, oxygen is not stable at B-, C-, D-, and H-sites and moves to the follow-

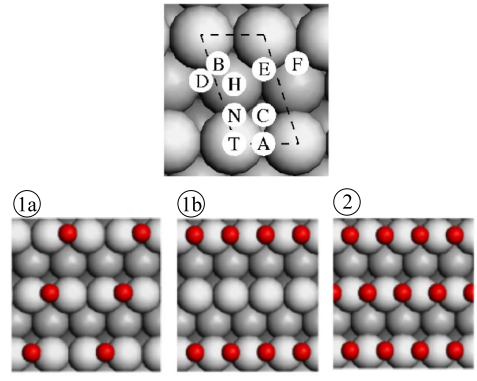

Figure 2. Top view of Ir(311) showing all binding sites at which O adsorption has been studied (top), as well as the most stable structures for different coverages (bottom): (1a and 1b) 0.5 ML, (2) 1 ML.

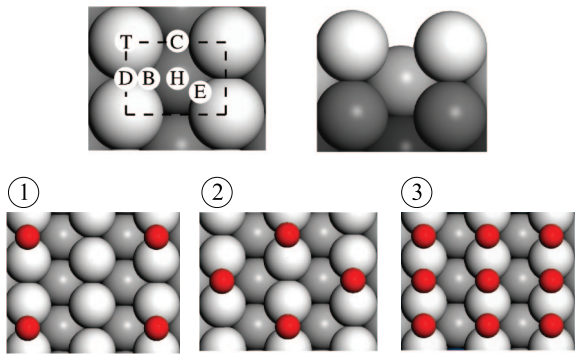

Figure 3. Top view of unreconstructed Ir(110) showing all binding sites at which O adsorption has been studied (top), as well as the most stable structures for different coverages (bottom): (1) 0.25 ML, (2) 0.5 ML, (3) 1 ML.

ing nearby positions during geometry optimization: B → A, C → A, D → E, and H → F.

Besides the adlayer arrangements discussed above, a coverage of 0.5 ML can also be achieved in a (2 × 1)-O structure (Figure 2-1b). Although in this configuration the preferred binding sites are again A-sites, the adsorption energy of 1.71 eV is 0.45 eV lower than with a (1 × 2) periodicity. This behavior can be explained by the relatively strong O−O repulsion since along each second substrate row all adjacent A-sites are occupied. Therefore, the row-pairing effect that was observed in case of the (1 × 2)-O structure and led to a reduced oxygen−surface distance is absent now, resulting in d(surface-O) = 1.49 Å. However, the Ir−O bond lengths are still 1.98 Å, showing that the nature of the bond remains (almost) unchanged. Again, with the (2 × 1) periodicity, F- and N-sites are less favorable positions compared to A-sites by 0.39 and 0.42 eV, respectively, and adsorption at B-, C-, D-, or H-sites is not stable at all.

Increasing the oxygen coverage to 1 ML, we still find the A-site to be most stable with a binding energy per adatom of 1.72 eV (see Figure 2-2), which is almost exactly the value obtained for 0.5 ML in a (2 × 1)-O structure. Therefore, we can conclude that even with 1 ML oxygen on the surface the O−O interaction is mainly due to adatoms being adsorbed on the same substrate row and that there is a negligible interaction between oxygen atoms of different rows. As for the previous cases the Ir−O bond length is again 1.98 Å and the substrate−O distance is 1.42 Å.

Ir(110)−O. Since we have recently reported detailed studies on clean and oxygen-adsorbed Ir(110) surfaces,[31] here we only give a brief summary.

Considering several ordered oxygen structures for each coverage, we always found the bridge site (D-site) to be preferred (see Figure 3). At 0.25 ML, only weak lateral adatom interactions can be expected. Therefore, the binding energy of 2.04 eV and bond length of d(Ir−O) = 1.97 Å which we calculated for a p(2 × 2)-O adlayer at the D-site should almost represent the zero-coverage limit. As a consequence of the strong interaction between oxygen and the surface, both Ir atoms to which the adatom binds are displaced by 0.07 Å away from the oxygen. This behavior, which we have already seen for the (311) surface and which seems to be more general for the late 5d elements, is also known as *row-pairing*. Significantly lower binding energies were obtained for C- (E_{bind} = 1.24 eV), B- (E_{bind} = 1.22 eV), and T-sites (E_{bind} = 1.16 eV).

At 0.5 ML, c(2 × 2)- and p(2 × 1)-O are both more stable than the p(1 × 2)-O adlayer, with binding energies per oxygen of 2.09 and 2.04 eV, respectively (oxygen at D-sites). The geometry of the most stable configuration [c(2 × 2)-O] shows good agreement with experimental measurements on the "oxidized" surface.[38] The expression "oxidized" is usually used since there is still an ongoing debate whether oxygen is adsorbed on the surface or forms a surface oxide. For the Ir−O distance and the vertical separation of the topmost substrate layers, we calculate values of d(Ir−O) = 1.97 Å and d_{12} = 1.31 Å, which should be compared to the corresponding experimental distances of 1.93 ± 0.07 and 1.33 ± 0.07 Å. This agreement is rather interesting since the experimentally prepared c(2 × 2)-O structure is usually thought of being adsorbed on an already formed surface oxide,[37−41] while in our calculations we assume a pure Ir(110)-(1 × 1) surface.

At a coverage of 1 ML, the D-site still remains energetically favored with binding characteristics of E_{bind} = 1.59 eV and d(Ir−O) = 1.99 Å. Interestingly, the top site (T-site) becomes the second favorable adsorption site (E_{bind} = 1.10 eV). Whereas at D-sites the Ir−O bond length is almost independent of the coverage, the adsorbates are closer to the surface plane by ~0.06 Å for both 0.25 and 0.5 ML compared to 1 ML. In addition, the calculated binding energy is significantly lower for 1 ML than for 0.25 and 0.5 ML by 0.45 and 0.50 eV, which is a direct consequence of a strong O−O repulsion.

Ir(110) Superstructure. Experimentally, it was found that the (110) faces of each nanopyramid consist of regular Ir(110)-(1 × 1) but also a more rough surface structure. On the basis of STM images and geometric considerations, Ermanoski *et al.* proposed the latter surface to be a stepped double-missing-row Ir(110) superstructure as shown on the left side of Figure 4.[23]

To better understand the oxygen adsorption on this rather complex surface and to add this structure to the full surface phase diagram (see next section), we performed DFT calculations on systems with up to four O atoms per unit cell, *i.e.*, θ = 1, ... , 4 ML.

Among the higher-symmetric surface sites indicated in the lower left model of Figure 4, a single oxygen atom per unit cell prefers to occupy F-sites (E_{bind} =2.19 eV), which are bridge positions located directly below the last Ir atom of each stepped row. Interestingly, binding on top of the row at the B-site, which again allows for bridge binding, results in an only slightly lower binding energy of 2.12 eV. Therefore, we

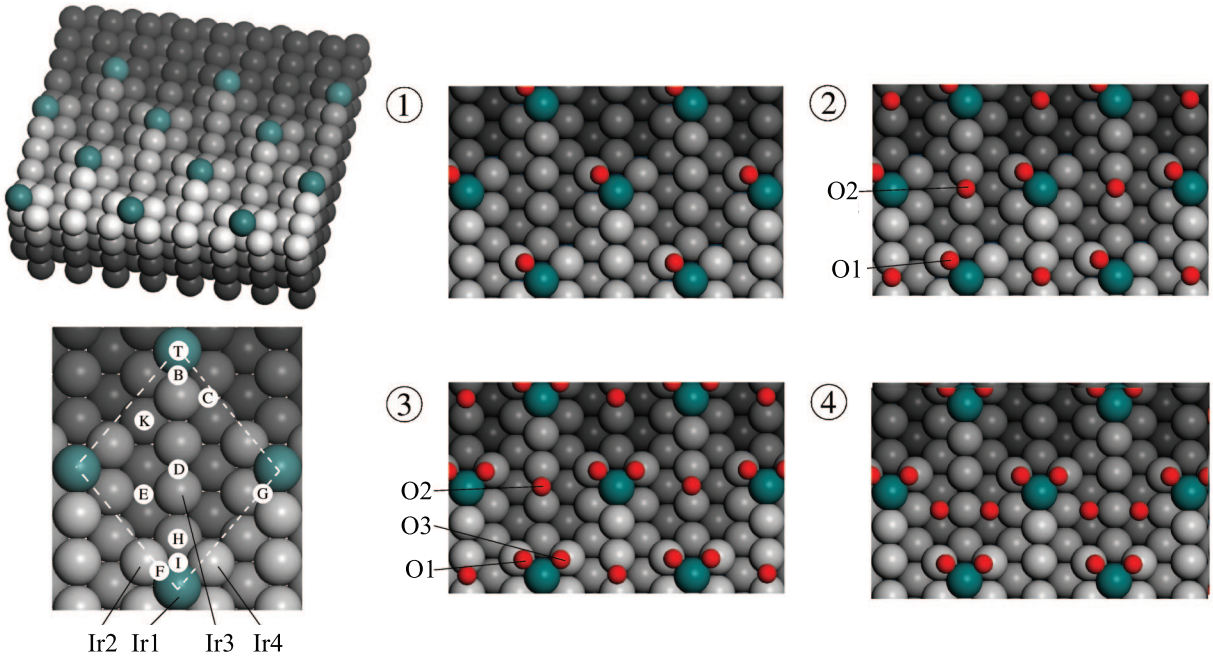

Figure 4. Top and perspective view of the "stepped double-missing-row" Ir(110) superstructure, showing all binding sites at which O adsorption has been considered (left), as well as the most stable structures for the different coverages (right): (1) 1 ML, (2) 2 ML, (3) 3 ML, (4) 4 ML.

can conclude that, on this stepped surface, oxygen is likely to be near the end of each row. However, there is a small barrier of ~0.2 eV to diffuse from B- to F-sites, which can be understood as a kind of Ehrlich–Schwöbel barrier. The next stable surface site is the D-site with a binding energy of 2.03 eV. Although this value is only 0.09 eV lower than the binding energy at the nearby B-site of the same row, diffusion of oxygen along the substrate rows is hindered by a relatively high barrier of >1 eV, thus again leading to a strong localization of adatoms around the row ends.

As a consequence of the rather extended surface unit cell of this structure, even two oxygen atoms per unit cell give a relatively low adsorbate density. Therefore, both oxygen atoms behave as almost independent adsorbates, and while the first oxygen occupies a F-site, the D-site remains for the second oxygen (see Figure 4-2). The weak O–O interaction is also confirmed by the binding energy per adsorbate of 2.11 eV, which is exactly the averaged value for binding a single oxygen per unit cell at F- and D-sites (see above). Only slightly weaker binding (E_{bind} =2.06 eV) is obtained with the more symmetric configuration of locating oxygen atoms at B- and D-sites.

Adding a third oxygen atom per unit cell does not change the binding site of the first two adsorbed atoms. Since most of the remaining vacant surface positions are lower-lying with respect to the surface plane, which are rather unfavorable surface sites, the third atom binds at the second of both possible F-sites (see Figure 4-3). For this F/F/D configuration, we calculated a binding energy of 1.96 eV per oxygen. Compared to the previous systems with one or two oxygen atoms per unit cell, this value is reduced, showing an increasing O–O repulsion. Caused by this relatively strong O–O repulsion, an adlayer configuration in which the spacing between the oxygen atoms is smaller (adsorbates at F-, F-, and B-sites) leads to an 0.53 eV lower average binding energy.

Finally, with the knowledge obtained already, we studied two possible arrangements with four oxygen atoms per unit cell: (1) at F-, F-, E-, and E-sites and (2) at E-, E-, C-, and C-sites. Since the O–O spacing in the first arrangement is on average larger than that of the second configuration, we find the first structure (see Figure 4-4) to be 0.76 eV more stable with an average binding energy of E_{bind} =1.31 eV.

(p_{O_2}, *T*) Surface Phase Diagram. The surface stabilities and oxygen binding energies for the different surfaces discussed in the previous sections and summarized in Table 2 [Ir(210), Ir(311)/Ir(31$\bar{1}$), Ir(110), and Ir(110) superstructure] were used to generate a full phase diagram for surface faceting (see Figure 5). There we distinguish between clean and oxygen-covered surfaces of (i) planar Ir(210), (ii) nanopyramids with (311), (31$\bar{1}$), and (110) regular faces, (iii) and nanopyramids with (311), (31$\bar{1}$), and (110) superstructure faces. The surface free energies γ for the faceted surfaces were calculated using the left side of eq 4 with the parameters for the partial surface areas and facet tilt angles summarized in Table 1. Each summand of this equation was evaluated by eq 5 where the main temperature and pressure dependence

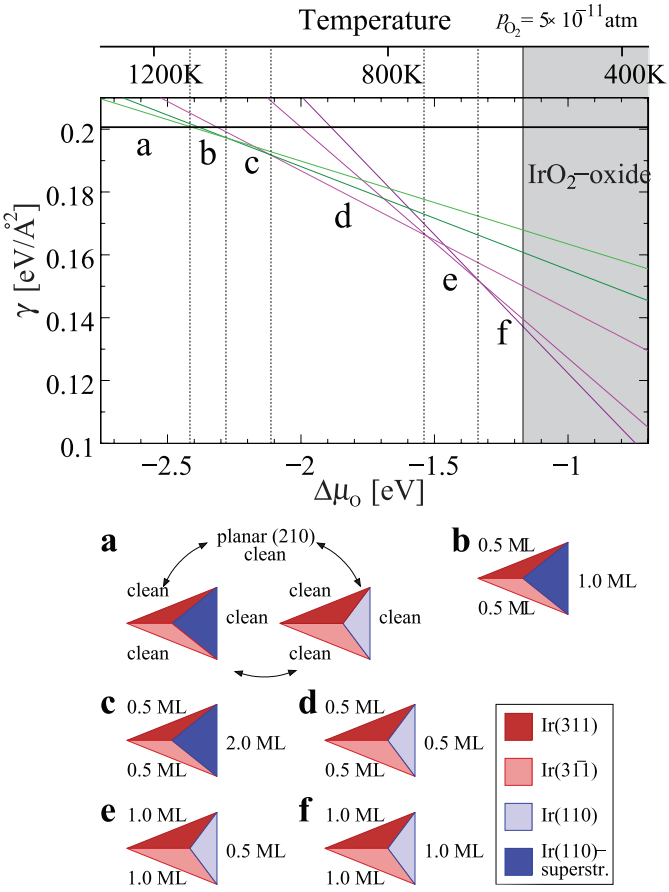

Figure 5. Surface phase diagram for the faceting of planar Ir(210), which shows the surface free energy γ as function of the oxygen chemical potential $\Delta\mu_O$. It combines clean and oxygen-covered planar Ir(210) as well as two types of three-sided nanopyramids: (311)/(31$\bar{1}$)/(110) regular (red lines) and (311)/(31$\bar{1}$)/(110) superstructure (green lines). To avoid confusion, only those phases (lines) are shown which are most stable (lowest lying) in their particular oxygen chemical potential range (labeled as a−f). The models below the diagram sketch the surface structures and oxygen coverages of these phases. Finally, for $p_{O_2} = 5 \times 10^{-11}$ atm, $\Delta\mu_O$ has been converted to a corresponding temperature scale given above the diagram.

is assumed to be dominated by the oxygen chemical potential (eq 6). As already mentioned above, this approach is based on the Herring condition, in which contributions from step-edges, kinks, and surface stress or strain are considered to be small. In order to construct the phase diagram, the total surface free energy was plotted against the oxygen chemical potential referenced by $\Delta\mu_O = \mu_O^{gas} - 1/2E_{O_2}^{tot}$. The chemical potential was then converted to a temperature scale for $p_{O_2} = 5 \times 10^{-11}$ atm since most facet formation experiments have been conducted under this pressure. The remaining discussion is based on this condition.

Although experimentally the coexistence of (110) regular and (110) superstructure was observed on the largest nanopyramids, we only consider the extremes in which the entire (110) faces of all pyramids are either (110) regular or (110) superstructure (see above).

Since our interest is in clean or oxygen-covered surface structures, we concentrate on the chemical potential range, where the IrO_2 bulk oxide (rutile-type structure) is not stable. To evaluate this condition, we calculated the corresponding heat of formation. The obtained value of $\Delta\mu_O = 0.93$ eV per oxygen atom is lower than the experimental value of $\Delta H_f^0 = 1.17$ eV/O, which is related to the known difficulties of density functional theory to accurately describe the O_2 molecule. Therefore, we shifted the $\Delta\mu_O$ scale to match the experimental value (see ref 31). This procedure only causes a modified reference for the oxygen chemical potential but does not change the conclusions, which are based on relative stabilities.

The surface phase diagram (Figure 5) shows that for temperatures above 1130 K no oxygen is adsorbed on the surface (phase a), which nicely agrees with the experimental value of 1150 K.[14] Although we find the lowest surface free energy for a faceted surface in which the nanopyramids consist of (311), (31$\bar{1}$), and (110) superstructure faces, the second type of nanofacets as well as planar nonfaceted Ir(210) are only 3−4 meV/Å^2 less stable. Since this energy difference is certainly within the accuracy of the calculations, from the surface free energies alone, no clear statement on the morphology of the clean surface is possible, that is why, in Figure 5, phase a has been assumed to show coexistence between clean planar and clean faceted Ir(210). However, so far we have neglected energy contributions from step-edges and kinks, which usually reduce the stability. Since these contributions, which will be in the same energy range, are only relevant for the faceted surfaces, we would predict the most stable clean surface to be planar Ir(210). This is also in agreement with experiment observations, finding clean planar Ir(210) at these high temperatures.

Below 1130 K, adsorption of oxygen takes place, causing the formation or stabilization of the nanofaceted surface. While facets formed at higher temperatures consist of (311), (31$\bar{1}$) and (110) superstructure faces (Figure 5, phases b and c), at lower temperatures, facets with (311), (31$\bar{1}$) and (110) regular faces are stable (phases d−f). Formation at even lower temperatures leads to an increasing oxygen coverage on the different facet faces but does not modify the structure. Finally, the IrO_2 bulk oxide appears as a stable phase for temperatures lower than 575 K.[42] Overall, we find the surface phases summarized in Table 3.

While we expect clean planar Ir(210) to be the stable phase at high temperatures, oxygen-covered planar Ir(210) might only be stable at temperatures below 1050 K and low adsorbate coverages. However, facets immediately become stabilized if there is enough oxygen on the surface to generate phase b or c of the phase diagram (Figure 5), which means 0.5 ML on both {311} faces and 1.0−2.0 ML on the Ir(110) superstructure phase. Assuming that during facet formation no oxygen desorbs from the surface, this would convert to ~0.9 ML (0.45 physical ML) on the planar Ir(210) substrate, which nicely agrees

TABLE 3. Temperature Ranges, Structures, and Oxygen Coverages of the Different Surface Phases Shown in the Phase Diagram in Figure 5 (Note: For All Surfaces, 1 ML Refers to 1 Adatom per Unit Cell, Whose Sizes Are Given in Table 1)

phase	temp range (K)	theoretically predicted structure
a	$1130 < T$	coexistence of planar and faceted Ir(210)
b	$1070 < T < 1130$	nanofacets with 0.5 ML oxygen on (311) and (31$\bar{1}$), and 1.0 ML on (110) superstructure
c	$1000 < T < 1070$	nanofacets with 0.5 ML oxygen on (311) and (31$\bar{1}$), and 2.0 ML on (110) superstructure
d	$740 < T < 1000$	nanofacets with 0.5 ML oxygen on (311) and (31$\bar{1}$), and 0.5 ML on (110) regular
e	$650 < T < 740$	nanofacets with 1.0 ML oxygen on (311) and (31$\bar{1}$), and 0.5 ML on (110) regular
f	$575 < T < 650$	nanofacets with 1.0 ML oxygen on (311) and (31$\bar{1}$), and 1.0 ML on (110) regular

with the critical coverage for faceting of ≥0.5 physical ML observed experimentally.[14,22] Moreover, the presence of the (110) superstructure face at temperatures of 1130 K > T > 1000 K is rather remarkable. On a planar Ir(110) surface, this superstructure is always less favorable than regular (110), but this is different for the faceted Ir(210) surface. There, the superstructure forms on the (110) side of the nanopyramids at higher temperatures, which is a consequence of the nonlinear dependency of the surface free energy on the tilt angle (see prefactors on the left side of eq 4) and the fact that the (110) faces of the nanopyramids are already tilted with respect to the (210) substrate. Again, this behavior is observed experimentally.[23]

In order to evaluate the influences coming from choosing the PBE exchange-correlation functional, we additionally calculated the most relevant surface structures with the LDA functional and generated the equivalent surface phase diagram. Comparison shows that with the LDA functional all phase transitions are shifted toward higher temperatures, without causing any changes in the ordering of the stable phases. Furthermore, the stability ranges, respectively, chemical potential ranges, of the different phases are almost the same with both xc functionals. Therefore, the conclusions drawn above are qualitatively independent of the xc functional.

CONCLUSIONS

We have applied DFT to study the stability of clean and oxygen-covered surfaces of Ir(210), (311), (110), and (110) superstructure, which are involved in the formation of nanopyramidal facets on Ir(210). For these surfaces, our calculations provide detailed information on the binding geometries and energetics of oxygen with different coverages. Using these energies in conjunction with the *ab initio* atomistic thermodynamics approach, we studied the surface stabilities on the basis of the corresponding surface phase diagram and found that for an oxygen partial pressure of 5×10^{-11} atm and temperatures lower than 1130 K, oxygen adsorbs on the surface, leading to the formation of the experimentally observed three-sided facets. While at higher temperatures these facets consist of (311), (31$\bar{1}$), and (110) superstructure faces, at lower temperatures, the (110) face is found to be unreconstructed, leading to (311)/(31$\bar{1}$)/(110) regular facets. Finally, lowering the temperature only leads to an increasing oxygen coverage at the different facet faces. While in this work we focused on the facet formation on Ir(210) induced by gaseous oxygen, future work will aim at the role of changing the adsorbate (*e.g.*, Cl) as well as the nature of the interface (solid−liquid).

COMPUTATIONAL PROCEDURE

In order to calculate the total energies of different surface structures, which are required to draw the full (p, T) surface phase diagram, we performed DFT slab calculations using the CASTEP code[24] with Vanderbilt-type ultrasoft pseudopotentials[25] and the generalized gradient approximation (GGA) exchange-correlation functional proposed by Perdew, Burke, and Ernzerhof (PBE).[26]

Layer-converged supercells consisting of 16-layer slabs for Ir(210), 11-layer slabs for Ir(311), 12-layer slabs for Ir(110), and 7-layer slabs for the Ir(110) superstructure were used to model oxygen adsorption with different coverages and adlayer structures. To decouple the interactions between neighboring slabs in the supercell geometry, repeated slabs were separated by a ~12 Å vacuum. For Ir(210), Ir(311), and Ir(110) superstructure, the bottom three layers and, for Ir(110), the bottom four layers were fixed at the calculated bulk structure, and the geometry of the remaining layers plus adsorbates was fully optimized (to <0.03 eV/Å). The Brillouin zones of the (1 × 1) surface unit cells of Ir(210), (311), (110), and (110) superstructure were sampled with 10 × 8, 14 × 8, 14 × 10, and 4 × 4 Monkhorst−Pack k-point meshes,[27] respectively. Finally, a plane-wave basis set with an energy cutoff of 340 eV was used.

Investigating the error sources related to slab thickness, vacuum size, plane-wave cutoff, and k-point mesh, we found the maximum overall error bar in the surface free energy to be <5 meV/Å^2 when using optimized values for each parameter.

Due to the known difficulties of DFT in correctly reproducing the binding energy of dioxygen, throughout this work, all oxygen binding energies are given with respect to half a gas-phase oxygen molecule. Therefore, for direct comparison with experiment, one has to add $^1/_2E_{bind}(O_2)$.

Acknowledgment. The authors gratefully acknowledge support from the German Academic Exchange Service (DAAD), the Fonds der Chemischen Industrie (FCI), and the Deutsche Forschungsgemeinschaft (DFG) within the framework of the Emmy-Noether-Program. The Rutgers coauthors acknowledge support from the U.S. Department of Energy (DoE), Office of Basic Energy Sciences.

REFERENCES AND NOTES

1. Madey, T. E.; Guan, J.; Nien, C.-H.; Dong, C.-Z.; Tao, H.-S.; Campbell, R. A. Faceting Induced by Ultrathin Metal Films on W(111) and Mo(111): Structure, Reactivity, and Electronic Properties. *Surf. Rev. Lett.* **1996**, *3*, 1315–1328.
2. Madey, T. E.; Nien, C.-H.; Pelhos, K.; Kolodziej, J. J.; Abdelrehim, I. M.; Tao, H.-S. Faceting Induced by Ultrathin Metal Films: Structure, Electronic Properties and Reactivity. *Surf. Sci.* **1999**, *438*, 191–206.
3. Chen, Q.; Richardson, N. V. Surface Faceting Induced by Adsorbates. *Prog. Surf. Sci.* **2003**, *73*, 59–77.
4. Chen, W.; Ermanoski, I.; Wu, Q.; Madey, T. E.; Hwu, H. H.; Chen, J. G. Adsorption and Decomposition of Acetylene on Planar and Faceted Ir(210). *J. Phys. Chem. B* **2003**, *107*, 5231–5242.
5. Chen, W.; Ermanoski, I.; Madey, T. E. Decomposition of Ammonia and Hydrogen on Ir Surfaces: Structure Sensitivity and Nanometer-Scale Size Effects. *J. Am. Chem. Soc.* **2005**, *127*, 5014–5015.
6. Chen, W.; Ermanoski, I.; Jacob, T.; Madey, T. E. Structure Sensitivity in the Oxidation of CO on Ir Surfaces. *Langmuir* **2006**, *22*, 3166–3173.
7. Bachelet, R.; Cottrino, S.; Nahélou, G.; Coudert, V.; Boulle, A.; Soulestin, B.; Rossignol, F.; Guinebretiere, R.; Dauger, A. Self-Patterned Oxide Nanostructures Grown by Post-Deposition Thermal Annealing on Stepped Surfaces. *Nanotechnology* **2007**, *18*, 015301.
8. Revenant, C.; Leroy, F.; Renaud, G.; Lazzari, R.; Létoublon, A.; Madey, T. E. Structural and Morphological Evolution of Co on Faceted Pt/W(111) Surface upon Thermal Annealing. *Surf. Sci.* **2007**, *601*, 3431–3449.
9. Song, K.-J.; Lin, J. C.; Lai, M. Y.; Wang, Y. L. Faceting Phase Transitions of Mo(111) Induced by Pd, Au and Oxygen Overlayers. *Surf. Sci.* **1995**, *327*, 17–32.
10. Danko, D. B.; Kuchowicz, M.; Kolaczkiewicz, J. Adsorbate-Induced Surface Rearrangement of the System Pd/Mo(111). *Surf. Sci.* **2004**, *552*, 111–122.
11. Kirby, R. E.; McKee, C. S.; Roberts, M. W. Low Temperature Oxygen and Activated Nitrogen Faceting of Ni(210) Surfaces. *Surf. Sci.* **1976**, *55*, 725–728.
12. Kirby, R. E.; McKee, C. S.; Renny, L. V. Faceting of Cu(210) and Ni(210) by Activated Nitrogen. *Surf. Sci.* **1980**, *97*, 457–477.
13. Sander, M.; Imbihl, R.; Schuster, R.; Barth, J. V.; Ertl, G. Microfacetting of Pt(210) Induced by Oxygen Adsorption and by Catalytic Co Oxidation. *Surf. Sci.* **1992**, *271*, 159–169.
14. Ermanoski, I.; Pelhos, K.; Chen, W.; Quinton, J. S.; Madey, T. E. Oxygen-Induced Nano-Faceting of Ir(210). *Surf. Sci.* **2004**, *549*, 1–23.
15. Gustafson, J.; Resta, A.; Mikkelsen, A.; Westerström, R.; Andersen, J. N.; Lundgren, E.; Weissenrieder, J.; Schmid, M.; Varga, P.; Kasper, N. Oxygen-Induced Step Bunching and Faceting of Rh(553): Experiment and *Ab Initio* Calculations. *Phys. Rev. B* **2006**, *74*, 035401.
16. Wang, H.; Chen, W.; Madey, T. E. Morphological Evolution in Oxygen-Induced Faceting of Re(12$\bar{3}$1). *Phys. Rev. B* **2006**, *74*, 205426.
17. Wang, H.; Chan, A. S. Y.; Chen, W.; Kaghazchi, P.; Jacob, T.; Madey, T. E. Facet Stability in Oxygen-Induced Nanofaceting of Re(12$\bar{3}$1). *ACS Nano* **2007**, *1*, 449–455.
18. Knight, P. J.; Driver, S. M.; Woodruff, D. P. Scanning Tunneling Microscopy Investigation of the Oxygen-Induced Faceting and "Nano-Faceting" of a Vicinal Copper Surface. *Surf. Sci.* **1997**, *376*, 374–388.
19. Vollmer, S.; Birkner, A.; Lucas, S.; Witte, G.; Wöll, C. Nanopatterning of Copper (111) Vicinal Surfaces by Oxygen-Induced Mesoscopic Faceting. *Appl. Phys. Lett.* **2000**, *76*, 2686–2688.
20. Reinecke, N.; Taglauer, E. The Kinetics of Oxygen-Induced Faceting of Cu(115) and Cu(119) Surfaces. *Surf. Sci.* **2000**, *454*, 94–100.
21. Walko, D. A.; Robinson, I. K. Energetics of Oxygen-Induced Faceting on Cu(115). *Phys. Rev. B* **2001**, *64*, 045412.
22. Ermanoski, I.; Swiech, W.; Madey, T. E. Nucleation and Coexistence of Nanometer-scale Facet Domains on O/Ir(210). *Surf. Sci.* **2005**, *592*, L299−L304.
23. Ermanoski, I.; Kim, C.; Kelty, S. P.; Madey, T. E. Atomic Structure of O/Ir(210) Nanofacets. *Surf. Sci.* **2005**, *596*, 89–97.
24. Segall, M. D.; Lindan, P. L. D.; Probert, M. J.; Pickard, C. J.; Hasnip, P. J.; Clark, S. J.; Payne, M. C. First-Principles Simulation: Ideas, Illustrations and the Castep Code. *J. Phys.: Condens. Matter* **2002**, *14*, 2717–2744.
25. Vanderbilt, D. Soft Self-Consistent Pseudopotentials in a Generalized Eigenvalue Formalism. *Phys. Rev. B* **1990**, *41*, 7892–7895.
26. Perdew, J. P.; Burke, K.; Ernzerhof, M. Generalized Gradient Approximation Made Simple. *Phys. Rev. Lett.* **1996**, *88*, 3865–3868.
27. Monkhorst, H. J.; Pack, J. D. Special Points for Brillouin-Zone Integrations. *Phys. Rev. B* **1976**, *13*, 5188–5192.
28. Blaha, P.; Schwarz, K.; Madsen, G. K. H.; Kvasnicka, D.; Luitz, J. *WIEN2k−An Augmented Plane Wave+Local Orbitals Program for Calculating Crystal Properties*; Technical University, Vienna, Austria, 2001.
29. Stull, D. R.; Prophet, H. *JANAF Thermochemical Tables*, 2nd ed. U.S. National Bureau of Standards, U.S. EPO: Washington DC, 1971.
30. Reuter, K.; Scheffler, M. Composition and Structure of the RuO_2 (110) Surface in an O_2 and CO Environment: Implications for the Catalytic Formation of CO_2. *Phys. Rev. B* **2003**, *68*, 045407.
31. Kaghazchi, P.; Jacob, T. First-Principles Studies on Clean and Oxygen-Adsorbed Ir(110) Surfaces. *Phys. Rev. B* **2007**, *76*, 245425.
32. Kittel, C. *Introduction to Solid State Physics*; Wiley: New York, 2005.
33. With 2 geometrical ML on Ir(210), the resulting atom density of 1.2×10^{15} atoms/cm^2 is around the experimental saturation coverage of 1×10^{15} atoms/cm^2,[14] therefore 2 geometrical ML correspond to approximately 1 physical ML.
34. Krekelberg, W. P.; Greeley, J.; Mavrikakis, M. Atomic and Molecular Adsorption on Ir(111). *J. Phys. Chem. B* **2004**, *108*, 987–994.
35. Lauterbach, J.; Boyle, R. W.; Schick, M.; Mitchell, W. J.; Meng, B.; Weinberg, W. H. The Adsorption of CO on Ir(111) Investigated with FT-IRAS. *Surf. Sci.* **1996**, *350*, 32–44.
36. Reinalda, D.; Ponec, V. Adsorption of CO on Evaporated Iridium Films, Studied with Infrared Reflection−Absorption Spectroscopy. *Surf. Sci.* **1980**, *91*, 113–130.
37. Taylor, J. L.; Ibbotson, D. E.; Weinberg, W. H. Chemisorption of Oxygen on the (110) Surface of Iridium. *Surf. Sci.* **1979**, *79*, 349–384.
38. Chan, C.-M.; Luke, K. L.; van Hove, M. A.; Weinberg, W. H.; Withrow, S. P. Structure of c(2 × 2) Oxygen Overlayer on Unreconstructed (110) Surface of Iridium. *Surf. Sci.* **1978**, *78*, 386–396.
39. Ladas, S.; Kennou, S.; Hartmann, N.; Imbihl, R. Characterization of the Oxygen Adsorption States on Clean and Oxidized Ir(110) Surfaces. *Surf. Sci.* **1997**, *382*, 49–56.
40. Bu, H.; Shi, M.; Rabalais, J. W. Coexisting (1 × 3) and (1 × 1) Structures in the O_2 Induced Phase-Change of Ir(110). *Surf. Sci.* **1990**, *236*, 135–142.
41. Bu, H.; Shi, M.; Boyd, K.; Rabalais, J. W. Scattering and Recoiling Analysis of Oxygen-Adsorption Site on the Ir(110)-c(2 × 2)-O Surface. *J. Chem. Phys.* **1991**, *95*, 2882–2889.
42. Peuckert, M. XPS Study on Thermally and Electrochemically Prepared Oxidic Adlayers on Iridium. *Surf. Sci.* **1984**, *144*, 451.